Energy & Environmental Science

PAPER

View Article Online
View Journal | View Issue

Cite this: *Energy Environ. Sci.*, 2014, **7**, 1117

Wiring zinc in three dimensions re-writes battery performance—dendrite-free cycling†

Joseph F. Parker, Christopher N. Chervin, Eric S. Nelson, Debra R. Rolison* and Jeffrey W. Long*

Received 15th November 2013
Accepted 22nd January 2014

DOI: 10.1039/c3ee43754j

www.rsc.org/ees

Zinc-based batteries offer a safe, inexpensive alternative to fire-prone lithium-based batteries, but zinc-based batteries do not exhibit sufficient rechargeability—yet. Breaking through the centuries-old roadblock to zinc-based rechargeable batteries requires rethinking the electrode structure in order to control how zinc converts to zinc oxide during battery discharge and how the oxide is reversed back to metal upon recharging. We address the problems of inefficient zinc utilization and limited rechargeability by redesigning the zinc electrode as a porous, monolithic, three-dimensional (3D) aperiodic architecture. Utilization approaches 90% (728 mA h g_{Zn}^{-1}) when the zinc "sponge" is used as the anode in a primary (single-use) zinc–air cell. To probe rechargeability of the 3D Zn sponge, we cycled Zn–*vs.*–Zn symmetric cells and Ag–Zn full cells under conditions that would otherwise support dendrite growth, and yet the Zn sponges remain dendrite-free after extensive cycling up to 188 mA h g_{Zn}^{-1}. By using 3D-wired zinc architectures that innately suppress dendrite formation, all zinc-based chemistries can be reformulated for next-generation rechargeable batteries.

Broader context

Zinc-based batteries have high practical specific energy (up to 400 W h kg^{-1} in Zn–air cells) and many advantages over Li-ion batteries: cheap and earth-abundant active materials, aqueous electrolytes, and reduced risks of catastrophic thermal runaway. Broader implementation of Zn-based batteries beyond certain niche markets is hindered by limited rechargeability and modest utilization of the theoretical discharge capacity of Zn (<60%). These performance drawbacks are inherent to the electrochemical behavior of Zn in alkaline electrolyte when the metal is structured in traditional anode form-factors (*e.g.*, powder composites or pastes). We address the problems of inefficient Zn utilization and limited rechargeability by redesigning the Zn electrode as a sponge—a porous, monolithic, three-dimensional (3D) aperiodic architecture. The enhanced cyclability characteristic of the Zn sponge design allows us to revisit the entire family of Zn-based batteries, but now with enhanced rechargeability and energy/power performance that meet or exceed state-of-the-art Li-ion batteries. Applications that require large stacks of many individual cells will be inherently safer with aqueous Zn-based rather than nonaqueous Li-based chemistry.

Introduction

Rechargeable lithium-ion batteries are today's energy-storage solution of choice for advanced technologies ranging from electronics to transportation. Numerous high-profile incidents of catastrophic failure[1–4] demonstrate the innate risks of this battery chemistry—flammable electrolytes in conjunction with O_2-releasing electrode materials—making now an opportune time to revisit historically safer, yet performance-limited battery chemistry, but reconfigured using a three-dimensional (3D) architectural perspective.[5,6] Zinc-based batteries offer a compelling alternative to Li-ion because of the extensive global reserves of Zn, the innate safety advantages that arise from using aqueous, nonflammable electrolytes, and specific energies that are comparable to or higher than Li-ion, for example with Ag–Zn (~150 W h kg^{-1}) and Zn–air (up to 400 W h kg^{-1}). Although long-established for primary (single-use) energy storage, Zn-based batteries have yet to make a significant impact for advanced technologies that demand extended charge–discharge cycling (*e.g.*, electric and hybrid electric vehicles).

The performance of conventional Zn-based batteries is often limited by the structure of the Zn anode, which typically comprises a powder-bed of Zn particles held together by a binder and infused with gel electrolyte. Although simple to fabricate and scale, this powder-composite electrode structure results in sub-optimal utilization of capacity, even on a single discharge—typically <60% of the 820 mA h g_{Zn}^{-1} theoretical capacity[7,8]—and when pushed through extended charge–discharge cycling, promotes irreversible passivation[9] and a propensity to form macroscopically long, electrical-short-inducing dendrites.[10] Prior efforts to improve Zn performance have focused on the use of soluble additives (*e.g.*, zincate,

US Naval Research Laboratory, Surface Chemistry Branch (Code 6170), 4555 Overlook Avenue SW, Washington, District of Columbia, USA. E-mail: rolison@nrl.navy.mil; jeffrey.long@nrl.navy.mil

† Electronic supplementary information (ESI) available. See DOI: 10.1039/c3ee43754j

Report Documentation Page

Form Approved
OMB No. 0704-0188

1. REPORT DATE	2. REPORT TYPE	3. DATES COVERED
2014		**00-00-2014 to 00-00-2014**

4. TITLE AND SUBTITLE	5a. CONTRACT NUMBER
Wiring zinc in three dimensions re-writes battery performance-dendrite-free cycling	5b. GRANT NUMBER
	5c. PROGRAM ELEMENT NUMBER
6. AUTHOR(S)	5d. PROJECT NUMBER
	5e. TASK NUMBER
	5f. WORK UNIT NUMBER
7. PERFORMING ORGANIZATION NAME(S) AND ADDRESS(ES) **US Naval Research Laboratory, Surface Chemistry Branch (Code 6170),4555 Overlook Avenue SW,Washington,DC,20375**	8. PERFORMING ORGANIZATION REPORT NUMBER
9. SPONSORING/MONITORING AGENCY NAME(S) AND ADDRESS(ES)	10. SPONSOR/MONITOR'S ACRONYM(S)
	11. SPONSOR/MONITOR'S REPORT NUMBER(S)

12. DISTRIBUTION/AVAILABILITY STATEMENT
Approved for public release; distribution unlimited

13. SUPPLEMENTARY NOTES
Energy Environ. Sci., 2014, 7,1117

14. ABSTRACT

15. SUBJECT TERMS

16. SECURITY CLASSIFICATION OF:			17. LIMITATION OF ABSTRACT	18. NUMBER OF PAGES	19a. NAME OF RESPONSIBLE PERSON
a. REPORT **unclassified**	b. ABSTRACT **unclassified**	c. THIS PAGE **unclassified**	**Same as Report (SAR)**	**14**	

inorganic acids,[11] and LiOH[12]) in the alkaline electrolyte or inclusion of solid-state additives (*e.g.*, Bi_2O_3,[13] HgO,[14,15] CdO,[16] PbO,[15] and complex ceramic oxides[17]) within the powder-bed electrode formulation. In all cases, the aim is to control the complex dissolution/precipitation dynamics of the Zn/Zn^{2+} redox reaction. Some of these strategies have improved cycling performance and Zn-specific capacity, yet often at the expense of introducing toxic and/or capacity-diluting components (for solid-state electrode additives).

We have redesigned the anode as a 3D architecture that comprises interconnected, co-continuous, Zn domains and void volume in a monolithic form factor ("sponge"). Our aim is to use the structural characteristics of the 3D architecture to control the Zn dissolution/precipitation processes absent the electrolyte and electrode additives noted above. The performance-enhancing features bestowed upon the Zn electrode, when transformed into a 3D porous architecture, are: (i) maintaining fully metallic, interconnected pathways within the core of the electrode structure such that long-range electronic conductivity is preserved throughout charge–discharge; (ii) amplifying the electrified interface in 3D such that current distribution is more uniform throughout the electrode structure; and (iii) restraining shape change in alkaline electrolytes by accelerating saturation/dehydration of zincate to ZnO within confined void-volume elements in the interior of the porous electrode. These features—innate to a 3D formulation of Zn—make it physically difficult to form macroscale dendrites because the conditions required for dendrite formation cannot be established.

We demonstrate herein that the Zn sponge architecture reaches ~90% utilization (728 mA h g_{Zn}^{-1}) when discharged in a primary Zn–air cell and that it can be electrochemically cycled without formation of macroscale dendrites, as evaluated in either "symmetric" test cells of Zn sponge *vs.* Zn@ZnO sponges (Zn core/ZnO shell) or Ag–Zn cells. The discharge capacity and cyclability of monolithic, 3D-wired Zn electrodes make them compelling candidates for implementation in next-generation Li-free rechargeable battery technology.

Results and discussion

Fabrication of Zn sponge electrodes

Monolithic Zn sponges are prepared by first casting and consolidating Zn powder emulsions, as adapted from a previously published protocol.[18] The mechanically fragile, mold-released sponge is strengthened by annealing under argon to 409 °C (mp_{Zn} 419.5 °C) to enhance necking between the <63 μm particles and then calcined at 665 °C in air to wrap the object in a ZnO shell that locks-in the porous shape as the metal core further fuses, yielding a monolithic sponge with the structural robustness required for routine handling.[19] This process is readily scalable and amenable to a variety of shapes and sizes as defined by the mold; the circular molds used for this study are 1.15 cm in diameter and yield 1–4 mm thick sponges. Scanning electron microscopy (SEM) verifies that sponges prepared by this protocol are highly porous structures with typical pore widths from 10–50 μm and surfaces covered by a coating of ZnO needles (Fig. 1); X-ray diffraction (XRD) confirms the presence of both Zn and ZnO (Fig. SI-1†).

The presence of ZnO, a semiconductor with reported electronic conductivity spanning 10^{-10} to 10^{-3} S cm^{-1},[20,21] introduces high charge-transfer resistance (>60 Ω cm^{-2}, the real impedance as normalized to the 1.04 cm^2 geometric area of the as-calcined sponge) and lowers the attainable discharge capacity. To convert the Zn@ZnO sponge to an all-metal Zn sponge, the ZnO shell is electroreduced in alkaline electrolyte in a flooded half-cell configuration using an automated two-step sequence of applying a constant reducing potential, interrupting to measure impedance, and repeating until the charge-transfer resistance is <0.2 Ω cm^{-2}. The loss of ZnO reflections in the XRD pattern (Fig. SI-1B†) confirms complete reduction to an all-Zn^0 sponge, while the ZnO needles associated with the pre-reduced sponges are micrographically absent (Fig. SI-1D†). The electroreduced sponges remain monolithic and mechanically strong with an average mass loss of 23.9 ± 3.4% (12 replicates; Table SI-1†), which arises from loss of O mass upon conversion of ZnO to Zn[22] plus dissolution of ZnO into the bulk electrolyte as soluble zincate complex ions,[23] primarily $Zn(OH)_4^{2-}$.

An enabling electrodic characteristic of the Zn sponge architecture is the ability to maintain low overpotential for Zn/Zn^{2+} redox even at high load (current density). Galvanostatic half-cell measurements reveal a linear dependence of the steady-state discharge voltage on applied current. Even at an imposed current of 250 mA (240 mA cm^{-2}), the overpotential required to maintain this discharge rate is still <+200 mV (see Fig. SI-2†). This low polarization falls well below the 500 mV voltage drop (from open-circuit) tolerated in conventional Zn-containing

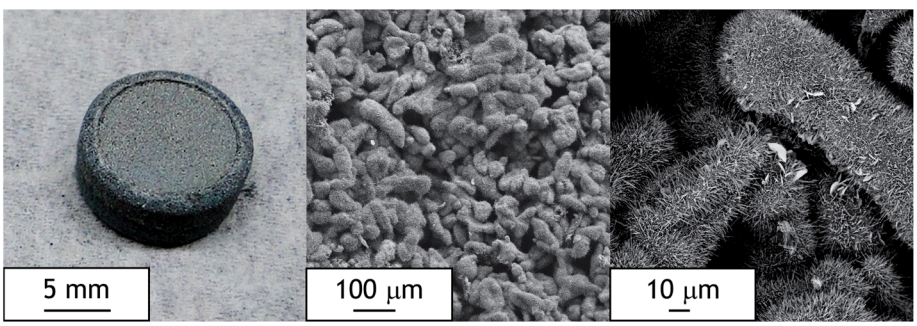

Fig. 1 Photograph (left) and scanning electron micrographs (middle and right) of a 3D Zn sponge after thermal processing in argon and then air, showing the porous network of the monolith and the needle-like ZnO surface structure at the individual Zn particles that comprise the sponge.

batteries, including Zn–air,[24] thus voltage loss at the Zn sponge anode will not be a limiting factor during operation.

Zn sponge anodes in primary batteries

As a preliminary test of Zn sponge performance, four Zn–air cells were constructed and discharged at ambient temperature to a 0.9 V limit at a high current load of 24 mA cm^{-2};[25–27] the average specific capacity delivered over this range is 694 ± 20 mA h g_{Zn}^{-1}, corresponding to a Zn utilization of 84.6% ± 2.4% expended over ~9 h (Table 1 and Fig. 2). Zinc–air cells were also discharged at lower rates (5 and 10 mA cm^{-2}), where comparable or slightly higher capacities (up to 728 mA h g_{Zn}^{-1}, equivalent to 89% Zn utilization) were achieved over multiday run times in conjunction with higher average cell voltages. Even at atypically high rates of discharge for a Zn–air battery, the sponge form-factor provides a substantial improvement in specific discharge capacity over standard Zn-powder composite anodes, which typically tap ~40% (ref. 28) to at best 50–60% of the theoretical specific capacity of Zn[7,8] when discharged at rates used to power hearing aids (<5 mA cm^{-2}).

Conventional Zn anodes, fabricated as composites of loosely connected Zn powder and polymer binder, underperform because interparticle electronic conductivity is interrupted during discharge as zincate ions dehydrate to resistive ZnO between the Zn particulate surfaces.[29,30] We attribute the increase in Zn utilization in the sponge architecture to the consequences of preserving long-range conductivity *via* the metallic Zn core within the sponge as ZnO coats the walls (Fig. 3); even after such deep discharge, cell resistance remains low at 2–3 Ω cm^{-2} (Fig. SI-3†). Dunn and co-workers previously noted the importance of maintaining an inner metallic core within a Zn@ZnO core–shell architecture during discharge, in that case using an open array of Zn rods as the anode in a 3D Zn–air microbattery.[31–33] High single-discharge Zn utilization has also been reported for mats of entangled Zn fibers tested as anodes for Zn–air cells[8] and with other 3D architectures specifically designed for use in microbatteries.[34–36] The scalability of the aperiodic sponge means that 3D Zn is not just for microbatteries anymore.

Rechargeability of Zn sponge anodes

The persistence of a metallic, 3D-wired Zn core within the sponge, which supports enhanced discharge capacity and specific energy in a primary Zn–air cell, should also promote electrochemical rechargeability, a breakthrough that will bring safe, low-cost Zn-based batteries to the performance level of rechargeable Li-ion batteries. For initial proof-of-concept of Zn sponge rechargeability, we used a test-bed cell with two sponge electrodes: Zn^0 sponge as the negative and Zn@ZnO sponge as the positive. This all-Zn two-electrode cell functions as an electroanalytical tool that allows one to put the 3D structure through its paces—we can force the inherent Zn dissolution/deposition reactions at rates one would rarely attempt in a battery. In addition to permitting high rates of charge–discharge, the symmetric cell circumvents the need for a complementary electrode that might otherwise limit performance at demanding current loads—*e.g.*, a bifunctionally catalyzed air cathode that can reduce and evolve O_2 in the case of a rechargeable Zn–air cell[37–39] or a Ag/Ag_xO cathode that can sustain high-rate charging.[40] Symmetric test cells are commonly employed in battery science for fundamental exploration of reversibility, interfacial characteristics, and the effect of additives on Li performance;[41,42] note that symmetric cells (*e.g.*, Li *vs.* Li or Zn *vs.* Zn) are not meant to attain voltages of relevance for practical batteries.

Zinc redox chemistry in alkaline electrolytes is a multiphase process involving Zn in both solid-state and solution-based

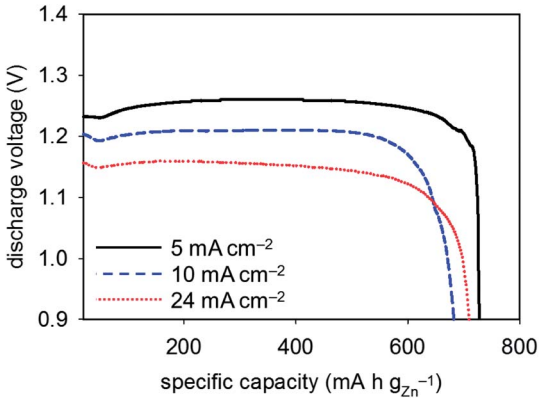

Fig. 2 Discharge curves of full-cell Zn–air batteries constructed using a fully reduced Zn sponge anode and an air-cathode composite of Ketjenblack carbon/cryptomelane/Teflon®. The discharge currents used are 5, 10, and 24 mA cm^{-2} and average discharge voltages of 1.25 V, 1.19 V, and 1.13 V, respectively, with the cells discharged to a cut-off voltage of 0.9 V *vs.* Zn (Table 1).

Table 1 Discharge characteristics as a function of discharge rate for Zn–air full-cells using 3D Zn-sponge anodes

Discharge current density[a] (mA cm^{-2})	Average cell discharge voltage[b] (V)	Specific capacity (mA h g_{Zn}^{-1})	Discharge time (h)	Specific energy density (W h kg_{Zn}^{-1})	Volumetric energy density[c] (W h L_{anode}^{-1})	Zn utilization (%)
5	1.25	728	37.2	907	1160	89
10	1.19	682	18.6	834	1070	83
24	1.13	709	9.0	809	1040	86
24	1.13	712	8.8	804	1030	87
24	1.13	672	8.0	761	979	82
24	1.11	684	8.2	764	983	83

[a] As normalized to the geometric footprint of the Zn sponge (its cross-sectional area); a discharge rate of 24 mA cm^{-2} corresponds to a C/10 rate (full capacity discharge in one hour is a 1 C rate). [b] The open-circuit voltage for these cells is consistently ≥1.4 V prior to discharge; cells were discharged to a cut-off cell voltage of 0.9 V. [c] The volumetric density was calculated from the cylindrical anode density of 1.29 ± 0.11 g cm^{-3}.

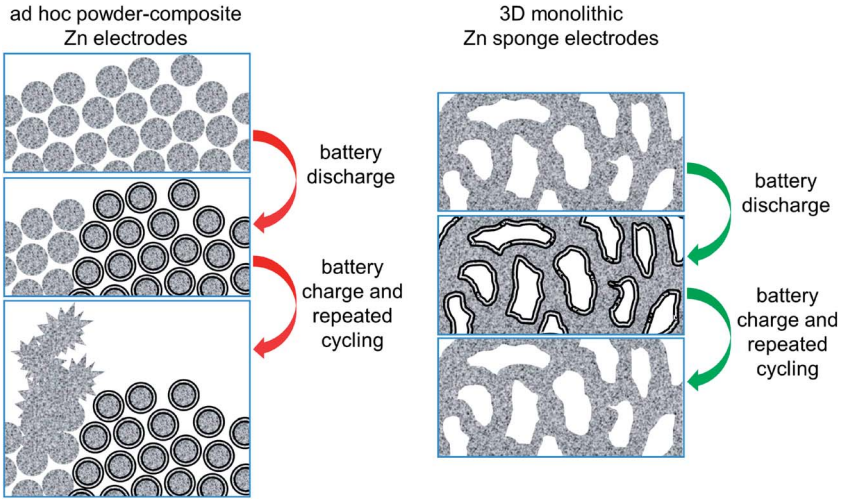

Fig. 3 Cross-sectional schematic of the dissolution–precipitation of ZnO in (left) conventional ad hoc powder-bed electrodes and (right) the 3D-wired Zn sponge electrode. Interparticle connectivity is lost in powder-composite electrodes leading to regions of high local current density and dendrite formation. The 3D Zn@ZnO core–shell architecture is maintained throughout charge–discharge, leading to high Zn utilization, controlled ZnO deposition within the void space, and diminished shape change upon cycling.

speciation. Upon discharge, Zn^0 is oxidized to Zn^{2+}, which reacts with hydroxide in the electrolyte to form a soluble series of zincate ions, primarily $Zn(OH)_4^{2-}$ (eqn (1)); subsequent dehydration of zincate forms resistive ZnO, not necessarily confined to just the electrified Zn surface, eqn (2) (Fig. 3). The relevant electrochemical reactions for each electrode in the symmetric cell upon application of negative current are:

discharge of bottom electrode:

$$Zn_{(s)} + 4OH^- \rightarrow Zn(OH)_4^{2-}{}_{(soln)} + 2e^- \quad (1)$$

$$Zn(OH)_4^{2-}{}_{(soln)} \rightarrow ZnO_{(s)} + H_2O + 2OH^- \quad (2)$$

charge of top electrode:

$$ZnO_{(s)} + H_2O + 2OH^- \rightarrow Zn(OH)_4^{2-}{}_{(soln)} \quad (3)$$

$$Zn(OH)_4^{2-}{}_{(soln)} + 2e^- \rightarrow Zn_{(s)} + 4OH^- \quad (4)$$

The symmetric Zn||Zn@ZnO cells were cycled at a high rate of ± 24 mA cm^{-2} within a ± 100 mV window[43–45] to 23% depth-of-discharge (DOD; 188 mA h g_{Zn}^{-1}, calculated with respect to the negative electrode). Although 23% DOD may seem modest, because of the relatively high specific energy of Zn–air, only 20–30% DOD is required—assuming Zn is 50–70% of total battery pack mass—to meet or exceed the specific energy metrics of commercial Li-ion batteries (Fig. SI-4†). During cycling, cell voltage toggles within a narrow voltage range ($\sim \pm 30$ mV), a voltage drop that arises primarily from resistive losses across the cell, before breaching the cut-off threshold after 45 charge–discharge cycles ($\sim$90 h of continuous cycling in a non-hermetically sealed cell;[46] Fig. 4). The post-cycled electrodes exhibit no obvious changes in dimension, shape, or monolithicity. Scanning electron micrographs show that the aperiodic 3D architecture of the electroreduced Zn sponge (Fig. 5A–C) is retained after serving as the negative electrode, with Zn/ZnO cycling products distributed homogenously at surfaces throughout the electrode structure (Fig. 5D–I). The positive Zn@ZnO sponge exhibits a compact morphology uniformly distributed throughout (Fig. SI-5†). We poised this Zn||Zn@ZnO symmetric cell (and replicates) to fail, *i.e.*, to be dendrite-prone: (i) without dendrite-suppressing additives or sophisticated charging methods;[47] (ii) without a complex separator system to serve as a physical barrier;[28] (iii) with high rates of cycling; and (iv) with both electrodes capable of launching dendrites. These conditions should promote formation of dendrites, and yet none are observed.

We also cycled symmetric cells to a lower DOD ($\sim$5%) in order to investigate the early-stage growth of Zn/ZnO products. After cycling to this lower DOD, micrometer-sized sprout-like deposits are uniformly distributed on the exterior and interior surfaces of the Zn sponge (Fig. 5D–F and SI-6,† respectively),

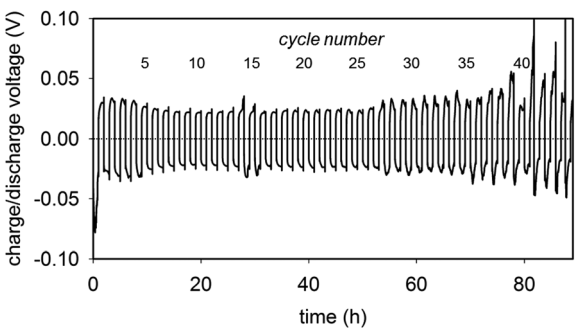

Fig. 4 The charge–discharge cycling data of a symmetrical Zn *vs.* Zn@ZnO cell for 45 charge–discharge cycles at ± 24 mA cm^{-2} to a depth-of-discharge of 23% relative to the bottom electrode ($\sim$90 h of continuous cycling). Cycling is programmed to terminate when the cell reaches ± 100 mV, which occurs around the 43rd cycle; the experiment is ended at the 45th cycle.

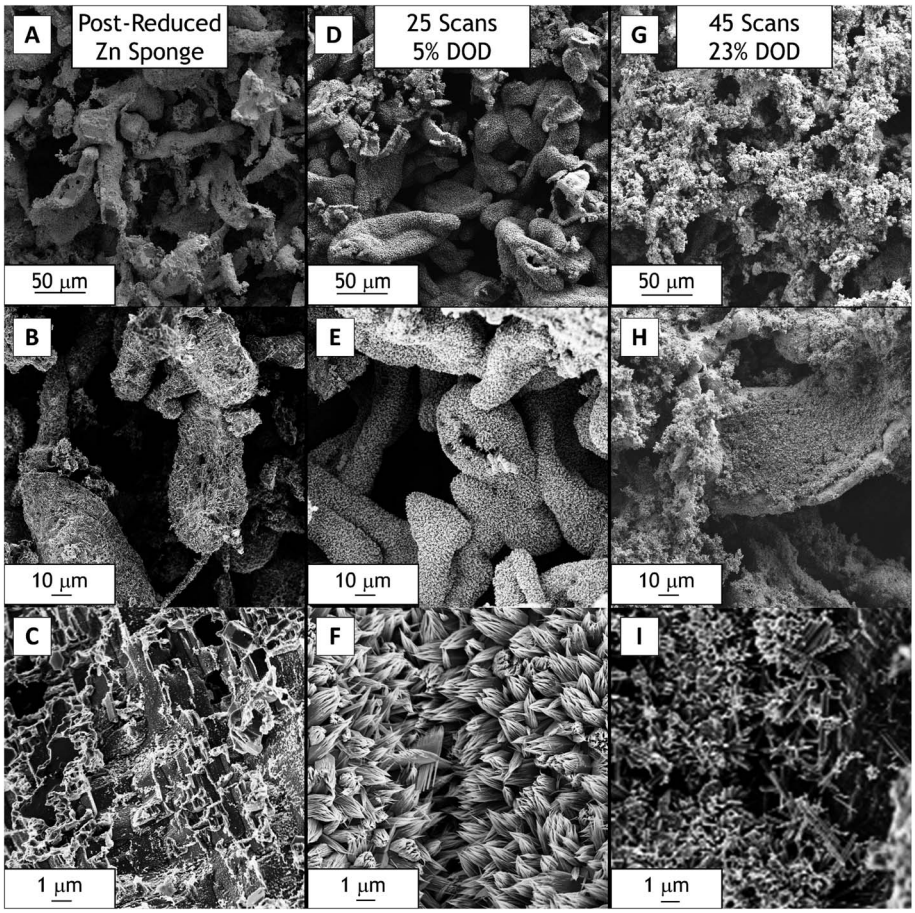

Fig. 5 Scanning electron micrographs demonstrating the changing morphology of the Zn sponge for (a–c) fully reduced, all-metal Zn and after charge–discharge cycling at (d–f) ±24 mA cm^{-2} for 25 times (to 5% depth-of-discharge) and (g–i) 45 times (to 23% depth-of-discharge). No obvious dendritic formations are found post-cycling.

signifying the manner in which the Zn surface restructures in the initial stages of charge–discharge. One can envision how such sprout-like structures, if inhomogenously distributed, would ultimately generate macroscale dendrites with extended cycling to greater DOD. Upon cycling Zn sponges to the deeper 23% DOD, the resulting Zn/ZnO coating exhibits a mixed morphology of micrometer-sized plates and spikes. We have neither observed any large-scale (>5 μm) dendritic growths in our SEM analysis of post-cycled Zn sponges nor measured any electrical characteristics that would indicate a dendrite-induced short circuit. The surface features we observe with extended cycling are similar to the morphology reported for 25% DOD single-discharge tests of pressed Zn-powder pellets, in which the uniform carpet-like deposition of ZnO obtained throughout the ~30% porous structure was attributed to achieving homogenous current distribution.[44]

A porous, well-wired Zn electrode, such as our Zn sponge, increases the electrified active area (calculated to be ~300 $cm^2\ g^{-1}$), so that although the nominal applied current density is relatively high (±24 mA cm^{-2} based on the 1.04 cm^2 geometric footprint), local current density[48] will be on the order of 10^{-1} mA cm^{-2}, 100× lower than that required to form Zn dendrites (typically >10 mA cm^{-2}).[45] While powder-bed electrodes may have similarly high surface area, the disruption in the long-range conductivity that occurs as individual particles are encased by resistive ZnO (Fig. 3) leads to zones of high local current density where dendritic spikes of Zn can form and grow long enough to pierce the separator and electrically short-circuit the battery.[7,45,49]

In addition to minimized local current density, we posit that the restricted void volume within the Zn sponge architecture lowers the likelihood of shape change. Upon oxidation, the concentration of zincate near the electrode surface rapidly exceeds its solubility, resulting in dehydration (eqn (2)) and precipitation as a ZnO shell that passivates the zincate-generating electrode surface (Fig. 3). This hypothesis is supported by our observation that the macroscale monolithic form is retained after cycling and the presence of homogenous Zn/ZnO deposits at the exterior and interior surfaces of the sponge (Fig. 5D–I; SI-5 and SI-6†); notably, we do not observe cycling products other than at the electrode surfaces such as solids that would occlude pores.

Secondary Ag–Zn cells

Primary silver–zinc (Ag–Zn) batteries have a long history of use in coin cells for small electronics and in larger form factors for

specialized military applications.[50,51] Silver–zinc batteries are distinguished by high specific power and a specific energy (~150 W h kg^{-1}) that approaches that of Li-ion batteries, but their broader use is limited by poor rechargeability. Following on our successful cycling of Zn sponges in the symmetric-cell configuration, we cycled prototype Ag–Zn cells comprising a fully reduced Zn sponge anode *versus* a conventional pressed-powder Ag_xO electrode.[40,52] After an initial conditioning cycle, the Ag–Zn cell was cycled at −5 mA cm^{-2} (discharge) and +3 mA cm^{-2} (charge, to accommodate the low-rate Ag/Ag_xO cathode)[40] targeting a capacity of 164 mA h $g_{Zn}{}^{-1}$ (20% DOD); specific capacity was maintained for 34 cycles, after which capacity rapidly faded (Fig. 6). As with the symmetric test cell, we find no evidence of electrical shorts after cycling, but attribute ultimate cell failure to other factors. Analysis of the post-cycled cell components revealed a blackened and resistive (*i.e.*, coated with Ag_2O) positive electrode current collector, which likely led to the cell failure for the Ag–Zn test case. Post-cycling SEM of the still-monolithic Zn sponge revealed a regular distribution of <1 μm needle-like deposits on the exterior and interior surfaces of the Zn sponge (Fig. SI-7†) with no indication of macroscale dendrite growth; this result confirms findings from the symmetric cell, but now in a practical battery configuration.

The Zn sponges described in this work represent a new class of monolithic anodes for Zn-based batteries that exhibit increased Zn utilization (~90%) in single-discharge use and inherently suppress dendrite formation under multiple charge–discharge cycles. The use of a 3D porous architecture to enable rechargeability in Zn anodes is based on a simple, scalable, readily manufacturable protocol, but the lessons derived from 3D Zn sponges can be extended to advanced manufacturing methods, such as 3D printing and selective laser sintering—as well as extended to metals other than Zn that are prone to dendritic morphology upon extended charge–discharge, including Li metal.

Materials and methods

All commercial reagents were used as received; water was purified to 18 mΩ cm (Barnstead MicroPure).

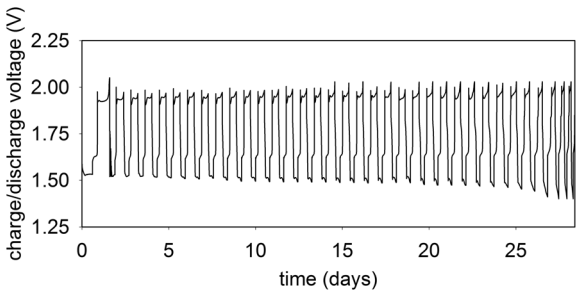

Fig. 6 The charge–discharge cycling data of Ag–Zn full cell for 36 cycles at −5 mA cm^{-2} (discharge rate) and +3 mA cm^{-2} (charge rate) to 164 mA h $g_{Zn}{}^{-1}$ (20% DOD relative to Zn; 28 days of continuous cycling). Cycling is programmed to terminate when the cell capacity falls below 50% of the initial capacity, which occurs at the 36th cycle.

Preparation of Zn sponges

In a typical synthesis, a vial is charged with Zn (6.0 g, Grillo-Werke AG, #G-6-0; also contains 300 ppm In and Bi to suppress hydrogen evolution) to which is added sodium dodecyl sulfate (6.3 mg, Aldrich), carboxymethylcellulose (0.253 g, Aldrich), water (1.027 mL), and decane (2.282 mL, Aldrich); the mixture is then stirred for 15 min. The resulting emulsion is pipetted into polyethylene molds of 1.15 cm diameter and allowed to settle and dry for at least 16 h. The fragile Zn powder monoliths are transferred to a tube furnace (Lindberg) and heated under flowing Ar at 2 °C min^{-1} to 409 °C and held at temperature for 2 h. The tube is then opened to ambient air and heated at 2 °C min^{-1} to 665 °C and held at temperature for 2 h. The tube is allowed to cool without any temperature control.

Electroreduction of post-heated Zn sponges

All electrochemical experiments were performed using a Gamry Reference 600 potentiostat. Half-cell measurements were carried out in 6 M KOH (Aldrich) using Pt-mesh counter and Zn-wire quasi-reference electrodes. A typical sequence begins with initial measurements of open-circuit potential (OCP) and electrochemical impedance. A reducing potential (−50 mV *vs.* Zn QRE) is applied for 30 min increments followed by measuring OCP. This process repeats until a stable OCP of <0 V is observed for 15 min and the real impedance falls below 500 mΩ cm^{-2}, indicating a metallic, device-ready anode.

Preparation of cryptomelane[27]

Manganese oxide sol–gel is formed by adding fumaric acid (386 mg; Aldrich) to a solution of $KMnO_4$ (1.58 g; Aldrich) in 50 mL of H_2O, mixed under vacuum for 8 min to facilitate the evolution of CO_2, and then left undisturbed to form the solid gel. The resulting gel is soaked in H_2O that is replaced 3–4 times per day to remove excess salt. The water is then replaced with 1 M H_2SO_4 briefly to oxidize Mn(III) centers and rinsed again with water for one more day. Finally, the gel is rinsed with acetone for 6 h and dried at 50 °C under flowing N_2. The solid MnO_x material remaining is heated to 300 °C for 2 h to form the cryptomelane 2 × 2 tunnel structure and then ground into a fine powder.

Preparation of carbon/cryptomelane/Teflon® (CCT) air cathodes

Ketjenblack carbon (AkzoNobel), cryptomelane, and an aqueous polytetrafluoroethylene mixture (60 : 40 Teflon®–water; Aldrich) are combined in a 4 : 1 : 1 mass ratio in a beaker and water is added until the dispersion can be easily stirred. The dispersion is stirred vigorously for 1 h and then dried at 50 °C under flowing N_2 to remove excess water. A 1.25 cm diameter disk of nickel mesh is pressed with a portion of the composite mixture to create a 1 mm thick cathode.

Evaluation of primary Zn–air cells

The electroreduced Zn sponges are submerged in 6 M KOH/PAA, prepared by mixing 100 mL of 6 M KOH with 100 g of

poly(acrylic acid) (Aldrich). The excess gel electrolyte is dabbed off and the Zn sponge is placed atop a tin-disk current collector. Tin is used as the negative electrode current collector because of its high overpotential for hydrogen evolution, stability in alkaline electrolyte, and galvanic compatibility with Zn.[26] An aqueous-compatible separator (Freudenberg) is placed between the anode and the carbon/cryptomelane/Teflon® (CCT) air cathode. Ni-mesh is used as a current collector to the air cathode with an extra Teflon® barrier placed between the air-cathode and the air-access hole of the cell. Initial OCP and impedance measurements are performed, followed by discharge at the chosen current density. When discharging at $\geq$10 mA cm^{-2}, a break-in discharge step of 5 mA cm^{-2} for 1 h is added prior to the run to ensure appropriate electrolyte permeation into the cathode.

Construction of two-electrode Zn@ZnO cells

Two Zn@ZnO core–shell sponges are prepared using the electroreduction treatment described above; however, the reduction step is limited to 15 min increments with impedance measurements after each step. At least one of the electrodes must contain a significant amount of ZnO, as evidenced by an OCP greater than 0 V *vs.* Zn QRE. Both electrodes are reduced until the R_{CT} falls to below 0.5 Ω cm^{-2}. For the experiment in Fig. 5D–F, the bottom (negative) electrode had an OCP of ~12 mV and the top (positive) electrode had an OCP of ~21 mV. For the experiment in Fig. 4 and 5G–I, the bottom electrode had an OCP of ~0 V (indicating nearly an all-metal state) and the top electrode had an OCP of ~32 mV. Both Zn@ZnO electrodes were used immediately after the electroreduction step while they remain infiltrated with 6 M KOH; however, the alkaline solution will saturate with zincate quickly upon the initial discharge. Both Zn@ZnO electrodes are placed atop tin current collectors with a nonwoven Freudenberg separator in between (Fig. SI-8†). Alternating current densities of ±24 mA cm^{-2} are applied until one of the steps crosses the ±100 mV threshold. We ascribe the onset of cell polarization and subsequent cycling termination to a combination of phenomena, including gas evolution, current-collector corrosion, and/or solvent evaporation as a result of our non-hermetically sealed cell, which all must be addressed prior to long-term cycling at higher depths-of-discharge. For post-cycling analysis, the electrodes are removed from the cell and rinsed thoroughly with 18 mΩ cm water. The cycled Zn sponges are then dried *in vacuo* overnight.

Cycling of Ag–Zn full-cells

Thermally cleaned silver mesh[53] (0.280 g, 1 cm^2) was placed in a die between two equal portions of 0.230 g of silver(II) oxide (AgO, Aldrich #223638) and pressed to 7000 psi. A Zn sponge electrode was fully electroreduced using the method described above, yielding a final mass of 0.222 ± 0.007 g. Tin and silver foil current collectors were used to connect the negative and positive terminals, respectively. The separator system included a Freudenberg® nonwoven separator on the zinc side, two layers of cellophane (Innovia films) to prevent silver migration,[54] and a layer of Celgard 3501 on the silver side. The first step was a galvanic discharge at 5 mA cm^{-2} to 328 mA h g_{Zn}^{-1} (40% DOD at Zn) followed by an exhaustive recharge at 3 mA cm^{-2} until broaching the 2.05 V cut-off voltage. Subsequent cycles were limited to 164 mA h g_{Zn}^{-1}.

Analytical characterization

Zinc sponges were analyzed at various stages throughout fabrication and experimentation using scanning electron microscopy (SEM; Carl Zeiss Leo Supra 55 scanning electron microscope, operated at 5 kV); the rinsed and dried sponge was mounted onto aluminium SEM stubs *via* nickel print. The X-ray diffraction patterns (XRD; Rigaku Smartlab) were collected for Zn sponges before and after electroreduction. The samples were ground using a mortar and pestle and placed in a recessed sample holder. The diffraction patterns were acquired in 0.02° intervals with 2 s dwell times using a Cu-Kα source operating at 40 kV and 44 mA.

Acknowledgements

This work was supported by the U.S. Office of Naval Research and the Defense Advanced Projects Agency (DARPA) and has been approved for Public Release, Distribution Unlimited. The views expressed are those of the authors and do not reflect the official policy or position of the Department of Defense or the U.S. Government. J.F.P. is a National Research Council – Naval Research Laboratory Postdoctoral Associate (2010–2014).

References

1 A. Cooper, Fire aboard empty 787 dreamliner prompts investigation CNN, 8 January 2013, http://www.cnn.com/2013/01/07/travel/dreamliner-fire/index.html.
2 A. Pasztor, Report on UPS jet's crash highlights cargo of batteries, Wall Street Journal, 3 April 2011, http://online.wsj.com/article/SB10001424052748703806304576241563707603894.html.
3 A. Heller, The G. S. Yuasa-Boeing 787 Li-ion battery: test it at a low temperature and keep it warm in flight, *The Electrochemical Society Interface, Editorial* (summer 2013).
4 R. A. Huggins, *J. Electrochem. Soc.*, 2013, **160**, A3001.
5 J. W. Long, B. Dunn, D. R. Rolison and H. S. White, *Chem. Rev.*, 2004, **104**, 4463.
6 D. R. Rolison, J. W. Long, J. C. Lytle, A. E. Fischer, C. P. Rhodes, T. M. McEvoy, M. E. Bourg and A. M. Lubers, *Chem. Soc. Rev.*, 2009, **38**, 226.
7 K. Harting, U. Kunz and T. Turek, *Z. Phys. Chem.*, 2012, **226**, 151.
8 X. Zhang, *J. Power Sources*, 2006, **163**, 591.
9 M. Minakshi and M. Ionescu, *Int. J. Hydrogen Energy*, 2010, **35**, 7618.
10 F. R. McLarnon and E. J. Cairns, *J. Electrochem. Soc.*, 1991, **138**, 645.
11 C. W. Lee, K. Sathiyanarayanan, S. W. Eom, H. S. Kim and M. S. Yun, *J. Power Sources*, 2006, **159**, 1474.

12 M. Minakshi, D. Appadoo and D. E. Martin, *Electrochem. Solid-State Lett.*, 2010, **13**, A77.
13 J. McBreen and E. Gannon, *J. Power Sources*, 1985, **15**, 169.
14 J. Goodkin, *U.S. Pat.* 3,493,434, 1970.
15 R. Shivkumar, G. Paruthimal Kalaignan and T. Vasudevan, *J. Power Sources*, 1998, **75**, 90.
16 A. Renuka, A. Veluchamy and N. Venkatakrishnan, *J. Appl. Electrochem.*, 1992, **22**, 182.
17 H. Huang, L. Zhang, W. K. Zhang, Y. P. Gan and H. Shao, *J. Power Sources*, 2008, **184**, 663.
18 J.-F. Drillet, M. Adam, S. Barg, A. Herter, D. Koch, V. M. Schmidt and M. Wilhelm, *ECS Trans.*, 2010, **28**, 13.
19 Alternative thermal treatments, such as heating solely under Ar or vacuum, yield zinc monoliths that are too fragile to handle.
20 P. Bonasewicz, W. Hirschwald and G. Neumann, *J. Electrochem. Soc.*, 1986, **133**, 2270.
21 H. Colak and O. Turkoglu, *Mater. High Temp.*, 2012, **29**, 344.
22 The mass of electroreduced zinc sponges are periodically spot-checked before assembling full cells and discharging; these values also fall within the established 23.9% mass-loss factor, which we use to calculate the specific capacity (mA h g_{Zn}^{-1}) of the Zn electrode.
23 V. K. Nartey, L. Binder and K. Kordesch, *J. Power Sources*, 1994, **52**, 217.
24 D. Linden, Zinc/air cells, *Handbook of Batteries*, 2nd edn, 1984, ch. 13.
25 The electroreduced Zn sponge is infiltrated with alkaline electrolyte and transferred to a nylon casing in which to package the full Zn–air cell; the sponge makes direct electrical contact to a tin current collector.[26] To complete the cell, we use a powder-composite air cathode comprising a ball-milled mixture of Ketjenblack carbon, nanoscale cryptomelane-type MnO_2,[27] and Teflon®, which has access to air *via* a 6 mm diameter hole on the top face of the prototype cell.
26 P. Bonnick and J. R. Dahn, *J. Electrochem. Soc.*, 2012, **159**, A981.
27 J. W. Long, K. E. Swider-Lyons, R. M. Stroud and D. R. Rolison, *Electrochem. Solid-State Lett.*, 2000, **3**, 453.
28 S. Müller, F. Holzer and O. Haas, *J. Appl. Electrochem.*, 1998, **28**, 895.
29 B. Aurian-Blajeni and M. Tomkiewicz, *J. Electrochem. Soc.*, 1985, **132**, 869.
30 H.-J. Park and S. Mho, *Anal. Sci.*, 1997, **13**, 311.
31 F. Chamran, Y. Yeh, H.-S. Min, B. Dunn and C.-J. Kim, *J. Microelectromech. Syst.*, 2007, **16**, 844.
32 B. Dunn, C.-J. Kim and S. Tolbert, *IEEE, MEMS 2010*, 2010, pp. 164–167.
33 F. Chamran, H.-S. Min, B. Dunn and C.-J. Kim, *IEEE Int. Conf. MicroElectromechanical Systems (MEMS '07)*, Kobe, Japan, 2007, pp. 871–874.
34 G. Sun, J. I. Hur, X. Zhao and C.-J. Kim, *J. Microelectromech. Syst.*, 2011, **20**, 876.
35 A. Armutlulu, Y. Fang, S. H. Kim, C. H. Ji, S. A. Bidstrup Allen and M. G. Allen, *J. Micromech. Microeng.*, 2011, **21**, 104011.
36 C. C. Ho, K. Murata, D. A. Steingart, J. W. Evans and P. K. Wright, *J. Micromech. Microeng.*, 2009, **19**, 094013.
37 C. N. Chervin, J. W. Long, N. L. Brandell, J. M. Wallace, N. W. Kucko and D. R. Rolison, *J. Power Sources*, 2012, **207**, 191.
38 J. W. Long, C. N. Chervin, N. W. Kucko, E. S. Nelson and D. R. Rolison, *Adv. Energy Mater.*, 2013, **3**, 584.
39 V. Neburchilov, H. Wang, J. J. Martin and W. Qu, *J. Power Sources*, 2010, **195**, 1271.
40 A. Himy, *Silver–zinc batteries: Phenomena and design principles*, Vantage Press, 1986.
41 P. C. Howlett, Y. Shekibi, D. R. MacFarlane and M. Forsyth, *Adv. Energy Mater.*, 2009, **11**, 1044.
42 J. C. Burns, L. J. Krause, D.-B. Le, L. D. Jensen, A. J. Smith, D. Xiong and J. R. Dahn, *J. Electrochem. Soc.*, 2011, **158**, A1417.
43 The voltage window was chosen because of the inherently fast electrode kinetics for Zn/Zn^{2+} redox[44,45] and demonstration that 3D Zn sponges exhibit low polarizability even at demanding loads (Fig. SI-2†); note that sustained voltages $>\pm100$ mV at ±24 mA cm^{-2} would indicate an accumulation of cell resistance or the onset of competing electrochemical processes (*e.g.*, hydrogen evolution).
44 Z. Nagy and J. O'M. Bockris, *J. Electrochem. Soc.*, 1972, **119**, 1129.
45 J. E. Oxley and C. W. Fleishmann, Improvement of zinc electrodes for electrochemical cells, first, second, and third quarterly reports, N66-13568, N66-16956, and N66-26870, 1965–1966.
46 We attribute the first cycle's higher potential of ~-80 mV to the initial higher impedance of the cell as the electrolyte penetrates the separator.
47 J. McBreen, *J. Electroanal. Chem.*, 1984, **168**, 415.
48 The specific electrified surface area was estimated using a 12.5 μm particle radius to establish a per-particle volume and surface area; using the density of Zn (7.14 g cm^{-3}) and the average mass of four Zn sponges to determine the number of particles per Zn sponge ($\sim4.3 \times 10^6$ particles) yields a corresponding surface area per gram of ~340 cm^2 g^{-1}
49 J. T. Kim and J. Jorné, *J. Electrochem. Soc.*, 1980, **127**, 8.
50 A. P. Karpinsky, B. Makovetski, S. J. Russell, J. R. Serenyi and D. C. Williams, *J. Power Sources*, 1999, **80**, 53.
51 J. Skelton and R. Serenyi, *J. Power Sources*, 1997, **65**, 39.
52 A. Himy, *Silver–zinc batteries: Best practices, facts and reflections*, Vantage Press, 1996.
53 J. F. Weaver and G. B. Hoflund, *Chem. Mater.*, 1994, **6**, 1693.
54 A. Henri, *Bull. Soc. Franc. Elec.*, 1941, **6**, 132.

SUPPLEMENTARY INFORMATION for

Wiring Zinc in Three Dimensions Re-Writes Battery Performance—Dendrite-Free Cycling

Joseph F. Parker, Christopher N. Chervin, Eric S. Nelson, Debra R. Rolison,* and Jeffrey W. Long*

Surface Chemistry Branch – Code 6170
U. S. Naval Research Laboratory
Washington, DC 20375, USA

Table SI-1 Control experiments from twelve nearly identical (mass/volume) Zn electrodes. Each Zn sponge was treated using the electroreduction process described in the main text. The results demonstrate that the mass loss associated with the electroreduction step to convert a Zn@ZnO sponge to a Zn^0 sponge is remarkably reproducible.

Zn sponge number	Initial open-circuit potential (mV vs. Zn QRE)	Initial mass (g)	Final mass (g) *	Mass loss (%)
1	22.6	0.379	0.298	21.3
2	27.4	0.361	0.268	25.7
3	27.6	0.406	0.297	26.7
4	30.5	0.404	0.307	24.1
5	32.9	0.336	0.246	26.8
6	35.3	0.423	0.323	23.7
7	36.0	0.396	0.331	16.5
8	37.1	0.369	0.281	23.8
9	37.1	0.413	0.315	23.7
10	38.5	0.394	0.294	25.3
11	39.3	0.326	0.262	19.6
12	100.1	0.378	0.268	29.1
			AVERAGE MASS LOSS	23.9
			STD. DEVIATION	3.4

* Electroreduced Zn sponges were washed thoroughly with 18 MΩ cm water and dried in vacuo before reweighing.

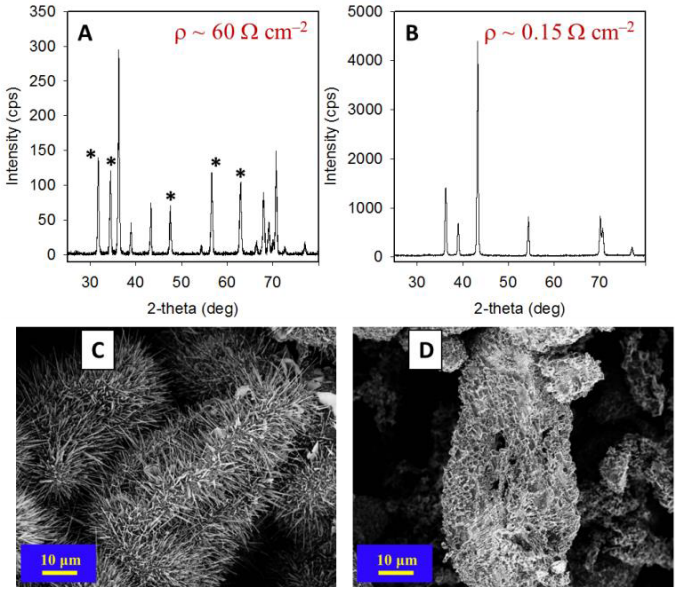

Fig. SI-1 Comparison of Zn sponges in (left) the as-prepared state and (right) after the electroreduction step. (A, B) X-ray diffraction demonstrating the loss of the ZnO content (∗) after reduction, with only reflections attributable to Zn metal remaining (Inset: values of real impedance, ρ, normalized to the 1.04-cm^2 geometric area of the sponge). (C, D) Scanning electron micrographs showing the removal of ZnO needles on the surface of the Zn walls in the sponge after electroreduction.

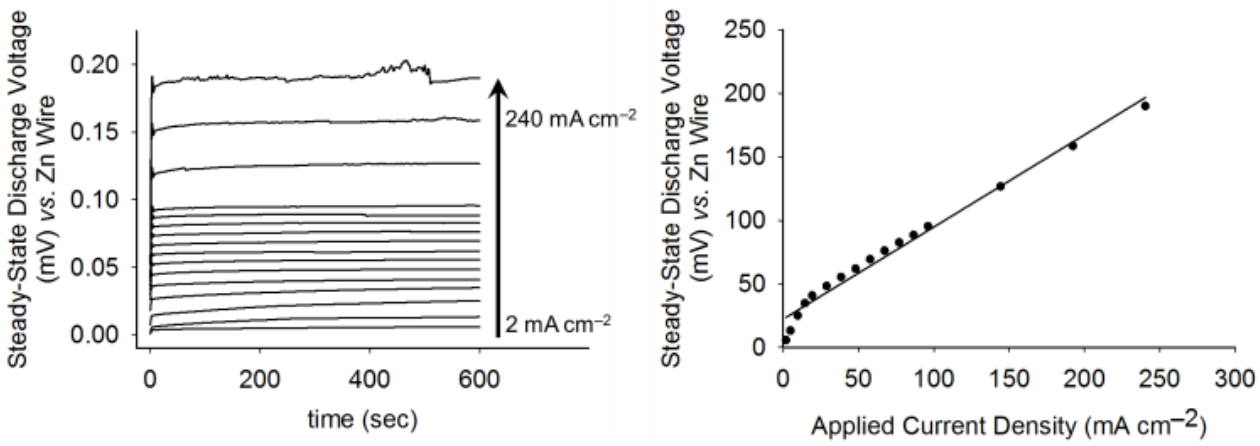

Fig. SI-2 (left) Steady-state discharge of a Zn sponge electrode in a flooded half-cell configuration in 6 M KOH with Zn wire quasi-reference and Pt-mesh counter electrodes. As applied current density is increased from 2–240 mA cm^{-2}, polarization remains < 200 mV and (right) scales linearly with applied load. The ability of the Zn sponge electrode to sustain such low polarization at very high current demands arises from the inherently fast electrode reaction (high exchange current density) for Zn^0/Zn^{2+} redox.

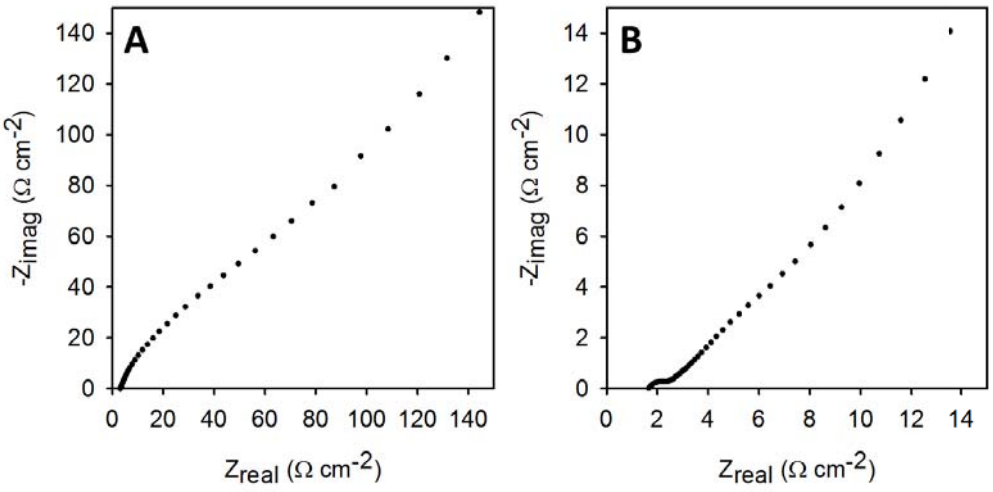

Fig. SI-3 Electrochemical impedance spectroscopy of a primary Zn–air full-cell (A) prior to discharge at 5 mA cm^{-2} to 83 % DOD and (B) post-discharged. The air cathode used in this test is a composite of Vulcan carbon/cryptomelane/Teflon®. The low cell resistance (2–3 Ω cm^{-2}) in both cases confirms that, while the majority of the Zn has been oxidized to ZnO, the electrical conductivity characteristic of metallic Zn remains indicating that the Zn core of the ZnO-coated architecture is maintained after a deep discharge.

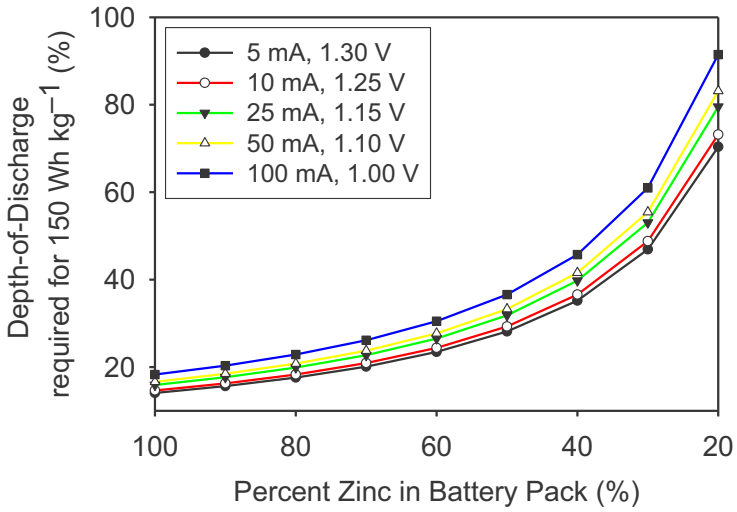

Fig. SI-4 Chart of depth-of-discharge (DOD) at Zn required to achieve 150 W h kg^{-1} (when projected into a Zn–air battery), a specific energy that rivals commercial Li-ion batteries, as a function of the Zn content of the battery pack at various loads (current demands). This analysis reveals that a fully engineered Zn–air battery, where Zn occupies 50–70% of the total pack mass would require 2–35% DOD at Zn.

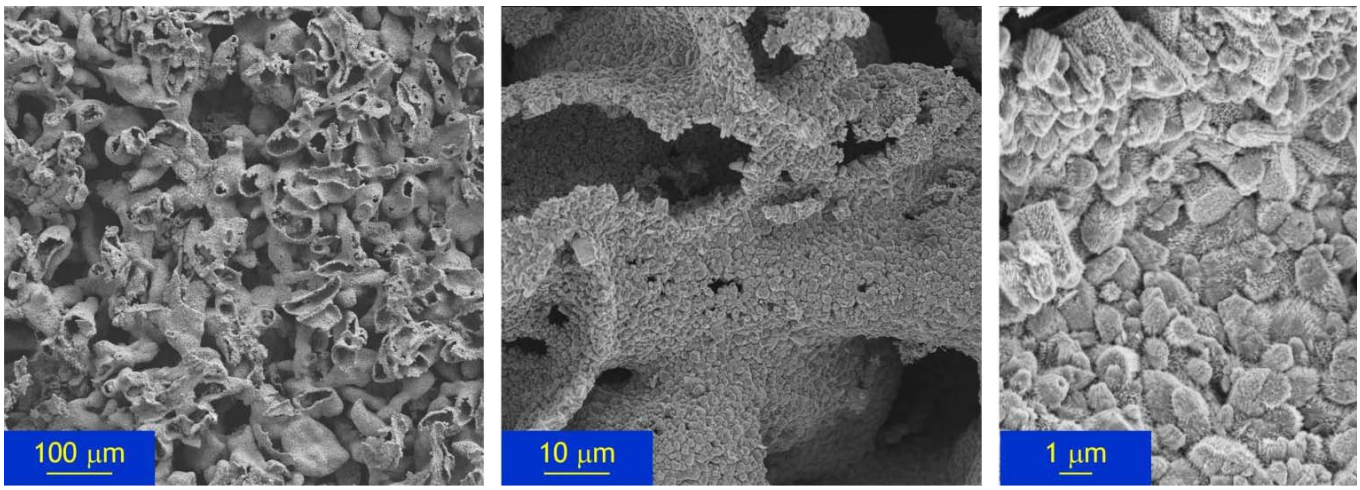

Fig. SI-5 Micrographs at various resolutions of the top (positive) Zn@ZnO sponge cycled at ±24 mA cm^{-2} for 43 scans (see Fig. 4 of main text for the cycling data and Fig. 5G–I for the opposing Zn@ZnO sponge micrographs). As a result of the differing masses of the two Zn@ZnO sponges in the model symmetrical cell, the top (positive) electrode was cycled to a lesser DOD (~9%) relative to the bottom (negative) electrode (~23%) presented in the main text. As expected, the morphology changes observed post-cycling are less pronounced in the top electrode because of the lower DOD. The deposition of compact Zn/ZnO products post-cycling occurs throughout the electrode structure and is consistent with uniformly distributed current density as a result of the well-wired sponge architecture, with no signs of dendrite formation. Note the revelation of the hollow character of the individual sintered Zn particles post-cycling.

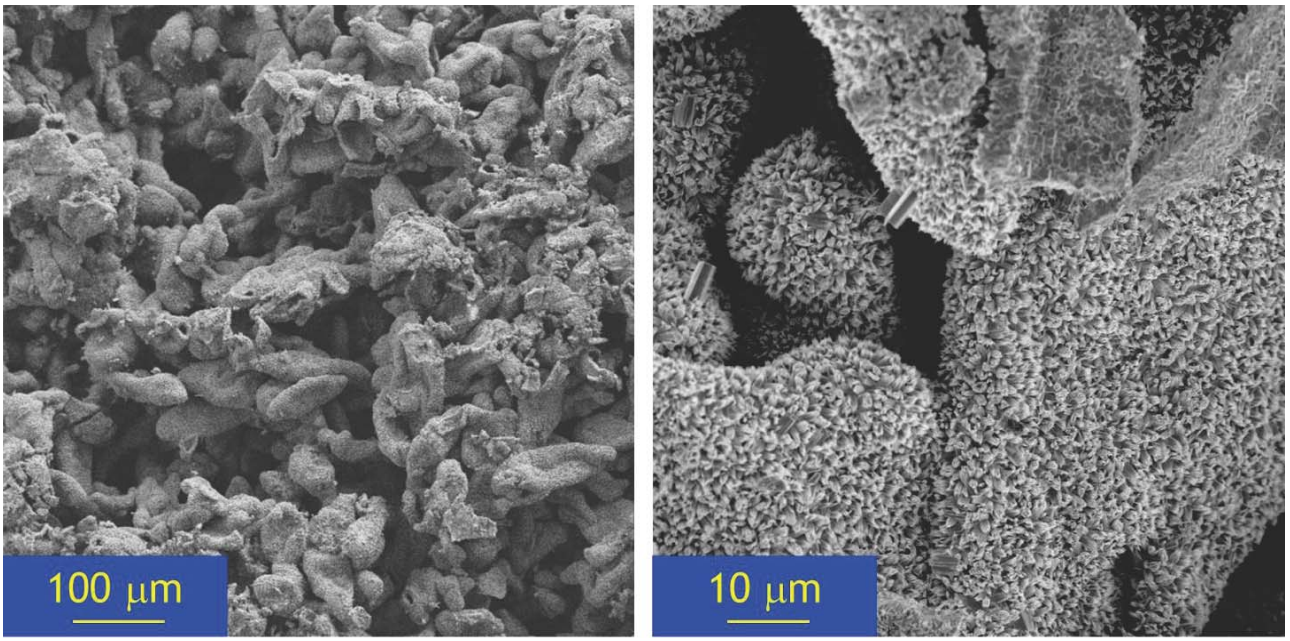

Fig. SI-6 Cross-sectional micrograph of a Zn@ZnO sponge cycled at ± 25 mA cm^{-2} to 5% DOD for 25 scans (see Fig. 5D–F of main text). Approximately 1 mm of the separator-facing edge of the bottom electrode was removed with a razor and re-imaged. The deposition of sprout-like Zn/ZnO products post-cycling occurs throughout the electrode structure and is not limited to the surface of the Zn@ZnO sponge.

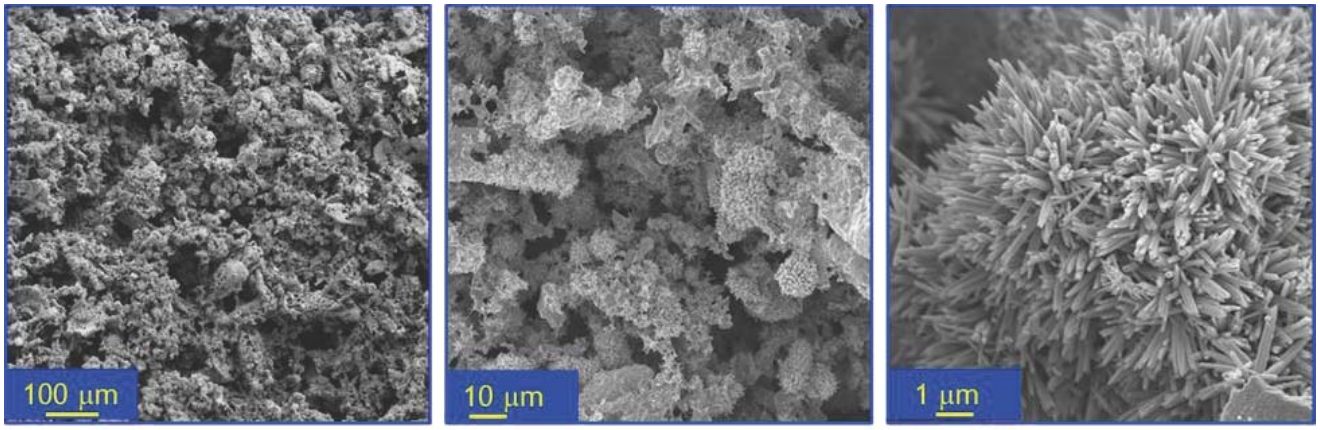

Fig. SI-7 Micrographs at various resolutions of the Zn sponge electrode cycled for 34 cycles in a Ag–Zn full cell at +5 mA cm^{-2} (discharge) and –3 mA cm^{-2} (charge)—see Fig. 6 of main text for the cycling data. As observed in the cycling data, the morphology observed after nearly a month of cycling reveals < 1 μm ZnO needles uniformly distributed throughout the electrode.

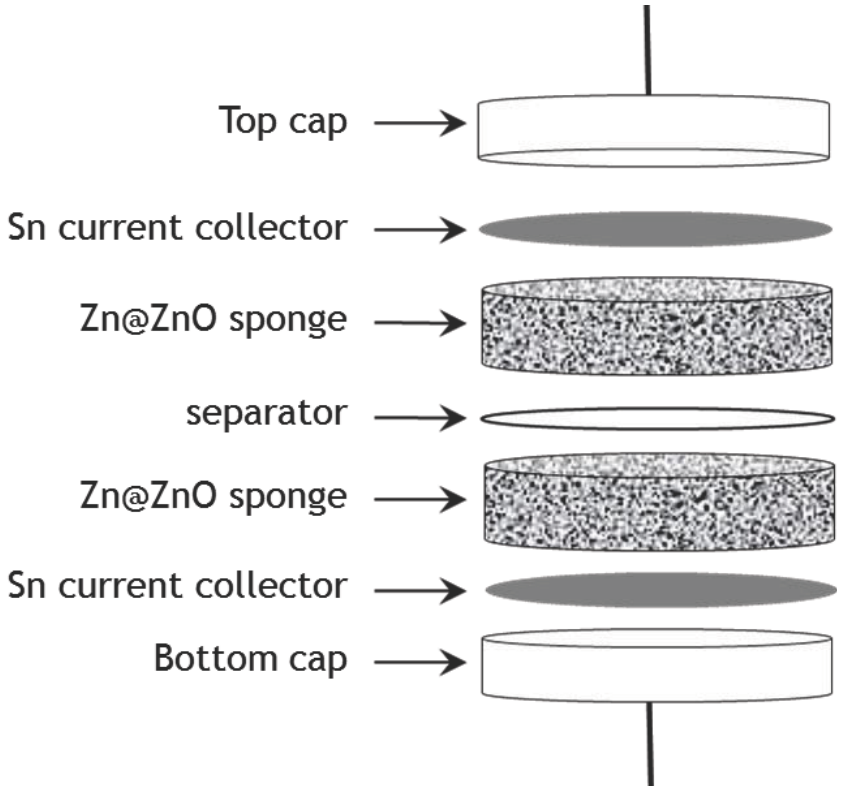

Fig. SI-8 Schematic of the Zn@ZnO symmetrical cell.